Progress In Electromagnetics Research, Vol. 105, 425–444, 2010

A TRI-BAND BANDPASS FILTER REALIZED USING TRI-MODE T-SHAPE BRANCHES

Y. Liu †

College of Information Science and Technology
Nanjing University of Aeronautics and Astronautics
Nanjing 210016, China

W. B. Dou

State Key Laboratory of Millimeter Waves
Southeast University
Nanjing 210096, China

Y. J. Zhao

College of Information Science and Technology
Nanjing University of Aeronautics and Astronautics
Nanjing 210016, China

Abstract—In this paper, we present a tri-band filter design using tri-mode T-shaped branches connected by $\lambda/4$ transmission lines. By analyzing the input admittance of a T-shape branch with commensurate electrical lengths, three resonant modes with two transmission zeros between are found and design formulas are derived. The filter can be regarded as a combination of three bandpass filters with only one set of coupling elements. To realize different bandwidths for each, the admittance slope of each resonating mode is set as required. A genetic algorithm is used in solving related equations to obtain the impedance of each line in a T-shape branch, followed by a final optimization. A three-pole tri-band filter having passbands of 0.6–0.9, 1.35–1.65 and 2.1–2.4 GHz, is designed, fabricated and measured with low passband insertion losses of < 0.7 dB and high rejection of > 60 dB between the passband regions. As a generalization, necessary to achieve a tri-band filter with arbitrary passbands, a non-commensurate version of the T-shape branch is introduced. An example filter design

Corresponding author: Y. Liu (lycloud1978@163.com).
† Also with State Key Laboratory of Millimeter Waves, Southeast University, Nanjing 210096, China.

is given with the passbands asymmetrically located at 0.7–1, 1.65–1.95, and 2.2–2.3 GHz. This technique is able to achieve good design flexibility with respect to bandwidth ratios. This is validated by studying the maximum impedance variations of a T-shape branch when the bandwidth ratios vary.

1. INTRODUCTION

Wireless communication has experienced rapid development in the last two decades, with several communication standards emerging, such as global system for mobile communication (GSM), personal communication system (PCS), and wideband code division multiple access (WCDMA), etc. These require modern RF front ends to support multi-standard operations. Also, RF coverage systems always need to combine several communication channels while rejecting unwanted signals. In [1], Lin presents a typical tri-band transceiver for general packet radio service (GPRS) applications. To satisfy the need of multi-band systems dual-band and tri-band filter have attracted much interest, and several techniques have been proposed. A coupling-matrix design procedure for tri-band filters in which cross-coupling that can achieve transmission zeros is used to split a wide passband into two or three separate passbands, is presented in [2]. However, in this method the passbands can not be widely spaced due to the bandwidth limitation of traditional coupled resonator filters.

A tri-band filter based on dual behavior resonators is reported [3] in which several bandstop structures are placed in parallel to construct the passbands. The reported performance is relatively poor, having higher insertion losses compared with the filters introduced here, as well as spurious responses.

In [4], a mixed bandpass-bandstop cicuit is used for dual-band filter realization, but is perhaps not suitable for realizing tri-band filters. In [5], a substrate integrated waveguide tri-band filter is described using the so-called "inverter coupled resonator sections". In [6, 7], split ring dual-mode and tri-mode resonators are used to design dual-band and tri-band filters. DGS resonating mode is used to introduce a second passband in [8, 9]. Lumped tri-band and quad-band filter networks are realized with coplanar elements in [10]. Stub loaded tri-mode resonators are used for tri-band filter design in [11].

Multi-mode stepped impedance resonators (SIRs) have now become popular in dual-band and tri-band filter design [12–20]. In [13–16], dual-mode SIRs and single mode resonators are combined to construct tri-band filters, or even quad-band filters, while, in [17–

20], tri-mode, tri-section SIRs are used for tri-band filter realization. However the internal coupling and external coupling schematics are relatively complex, and difficult to design with coupling coefficients satisfying all the passband requirements. (Often one needs two or more sets of coupling elements for filter implementation). SIR tri-band filters always have narrow passbands unless very thin lines and narrow coupling spaces are used, and these are difficult to manufacture.

A T-shaped composite resonator was proposed in [21] for realizing dual-band filters. On the other hand, in this paper, we introduce a "Tri-mode T-shape branch" consisting of a connecting line terminating in short- and open-circuited stubs connected in parallel. A tri-band filter can be designed by replacing the short-circuited stubs of traditional stub filters with this branch circuit. It has the advantage of enabling wide bandwidths to be realized. Also because the three passbands are transformed from the same distributed prototype low-pass filter, it is not necessary to design two or three sets of coupling elements to satisfy three sets of coupling coefficients simultaneously, but only to design the admittance slopes of all resonating modes to achieve the required bandwidths. Although the connecting lines can not realize wideband J inverters, we obtain good performance by optimizing the parameters of each T-shape branch. This tri-mode structure also introduces two transmission zeros between the three passbands to achieve high isolation.

This paper is organized as follows. In Section 2, the resonating modes and transmission zeros of the commensurate T-shape branch are analyzed and design formulas are derived, with a design procedure for realizing tri-band filters. Section 3 gives an example design, with a comparison between the simulation and measured results. In Section 4, non-commensurate T-shape branches are used to obtain arbitrary center frequencies and bandwidths, and a genetic algorithm is utilized to solve this relatively complex problem. Again, a design example together with simulation and measured results is given. Conclusions are presented in Section 5.

2. THEORY AND DESIGN OF THE TRI-BAND FILTER

2.1. The Commensurate T-shape Branch and Its Resonating Modes

Figure 1 gives the topology of the required "T-shape branch". It consists of an input transmission line with characteristic impedance Z_1 followed by short and an open-circuited stubs having characteristic impedances of Z_s and Z_o respectively. For simplicity, initially the case where all lines are commensurate is treated, and we set the electrical

lengths to be θ. We obtain:

$$Y_{in1} = \frac{j\tan(\theta)}{Z_o} - \frac{j\cot(\theta)}{Z_S} \tag{1}$$

and

$$Z_{in} = \frac{1}{Y_{in}} = Z_1 \cdot \frac{1/Y_{in1} + jZ_1\tan(\theta)}{Z_1 + j\tan(\theta)/Y_{in1}} = Z_1 \cdot \frac{1 + \frac{Z_1}{Z_s} - \frac{Z_1}{Z_o}\tan^2(\theta)}{j\left(\left(\frac{Z_1}{Z_o}+1\right)\tan(\theta) - \frac{Z_1}{Z_s}\cot(\theta)\right)} \tag{2}$$

Considering the denominator of Equation (2), we find two poles for the input impedance, corresponding to the resonant frequencies, by setting:

$$\left(\frac{Z_1}{Z_o} + 1\right)\tan(\theta) - \frac{Z_1}{Z_s}\cot(\theta) = 0 \tag{3}$$

leading to:

$$\theta_{r1} = \arctan\left(\sqrt{\frac{Z_1 Z_o}{Z_s(Z_1 + Z_o)}}\right) \tag{4a}$$

$$\theta_{r2} = \pi - \arctan\left(\sqrt{\frac{Z_1 Z_o}{Z_s(Z_1 + Z_o)}}\right) \tag{4b}$$

The two corresponding resonant frequencies are:

$$f_{rn} = \frac{c\theta_{rn}}{2\pi L\sqrt{\varepsilon_{eff}}} \quad n = 1, 2 \tag{5}$$

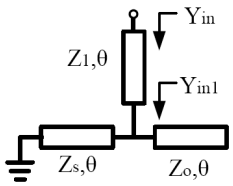

Figure 1. Circuit topology of the tri-mode T-shape branch (commensurate case).

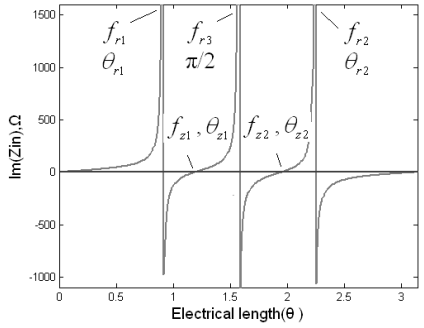

Figure 2. Plot of input reactance of the commensurate T-shape branch when the electrical length θ (radian) varies.

here L is the physical length of the commensurate lines, ε_{eff} is the effective dielectric constant of the transmission lines, and c is the velocity of light. For simplicity, we assume that the value of ε_{eff} does not vary for different impedance levels.

The third resonance occurs at $\theta = \pi/2$, from which Equation (2) can be written as:

$$Z_{in} = \frac{jZ_1^2 \tan(\theta)}{Z_1 + Z_o} \tag{6}$$

and the resonant frequency is:

$$f_{r3} = \frac{c}{4L\sqrt{\varepsilon_{eff}}} \tag{7}$$

Also two transmission zeros will occur when we set the numerator of (2) to zero:

$$1 + \frac{Z_1}{Z_s} - \frac{Z_1}{Z_o}\tan^2(\theta) = 0 \tag{8}$$

We get

$$\theta_{z1} = \arctan\left(\sqrt{\frac{(Z_1 + Z_s)Z_o}{Z_s Z_1}}\right) \tag{9a}$$

$$\theta_{z2} = \pi - \arctan\left(\sqrt{\frac{(Z_1 + Z_s)Z_o}{Z_s Z_1}}\right) \tag{9b}$$

The two transmission zeros are located at:

$$f_{zn} = \frac{c\theta_{zn}}{2\pi L\sqrt{\varepsilon_{eff}}} \quad n = 1, 2 \tag{10}$$

By comparing the values, we find:

$$\theta_{r1} < \theta_{z1} < \pi/2 < \theta_{z2} < \theta_{r2} \tag{11}$$

Thus we know:

$$f_{r1} < f_{z1} < f_{r3} < f_{z2} < f_{r2} \tag{12}$$

From (12), we know that the two transmission zeros are located between the three resonating frequencies, and high isolation between passbands will be achieved.

The distribution of the these frequencies is shown in the plot of Fig. 2, showing Z_{in} as a function of θ varying from 0 to π.

These resonant frequencies will be used to produce passbands. At f_{r1} and f_{r2}, the T-shape branch can be made equivalent to a shunt

parallel resonator with an admittance slope related to the passband bandwidth. The admittance slope is given by

$$\begin{aligned} b_n &= \frac{dB_{in}}{d\omega} = \frac{d\mathrm{Im}(Y_{in}(\omega))}{d\omega}\,|_{f=f_{rn}} = \frac{d\mathrm{Im}(Y_{in}(\omega))}{d\tan(\theta)}\frac{d\tan(\theta)}{d\omega}\,|_{f=f_{rn}} \\ &= \frac{d(1/Z_{in}(\tan(\theta))}{d\tan(\theta)}\sec^2(\theta)\frac{\pi}{2\omega}\,|_{f=f_{rn}} \\ &= \frac{\sec^2(\theta)}{4Z_1 f_{r3}}\frac{(k_1k_3-3k_2k_4)+k_1k_4\tan^2(\theta)+k_2k_3\cot^2(\theta)}{(k_3-k_4\tan^2(\theta))^2}\,|_{f=f_{rn}} \\ &= \frac{L\sqrt{\varepsilon_{eff}}(1+k_5)}{2\pi Z_1 c}\frac{(k_1k_3-3k_2k_4)+k_1k_4k_5+k_2k_3/k_5}{(k_3-k_4k_5)^2} \quad n=1,2 \end{aligned} \tag{13}$$

where θ can be expressed as:

$$\theta = \frac{\omega L\sqrt{\varepsilon_{eff}}}{c} = \frac{\pi}{2}\frac{f}{f_{r3}} \tag{14}$$

and:

$$k_1 = 1 + Z_1/Z_o \tag{15a}$$
$$k_2 = Z_1/Z_s \tag{15b}$$
$$k_3 = 1 + Z_1/Z_s \tag{15c}$$
$$k_4 = Z_1/Z_o \tag{15d}$$
$$k_5 = \frac{Z_1 Z_o}{Z_s(Z_1+Z_o)} \tag{15e}$$

We should note that b_1 is equal to b_2.

At f_{r3}, the T-shape branch is equivalent to a short-circuited stub with the characteristic impedance

$$Z_c = Z_1^2/(Z_1+Z_0) \tag{16}$$

2.2. Tri-band Filter Design

Traditional bandpass filters can be derived from distributed lowpass prototype filters such as that shown in Fig. 3(a) by using lowpass to bandpass transformations giving the filter of Fig. 3(b) or by using Richard's transformation to give the stub filter of Fig. 3(c). The bandwidths are determined by the admittance slope of each resonator.

For convenience we can set all the J inverters of a distributed prototype lowpass filter to be at the same impedance level, so that

$$J_{01} = J_{N-1,N} = Y_0 \tag{17}$$

$$J_{12} = J_{23} = \ldots = J_{N-1,N} = \begin{cases} Y_0 & N \text{ is even} \\ Y_0\sqrt{g_0 g_{n+1}} & N \text{ is odd} \end{cases} \tag{18}$$

$$C_{a1} = C_{aN} = Y_0 g_0 g_1 \tag{19}$$

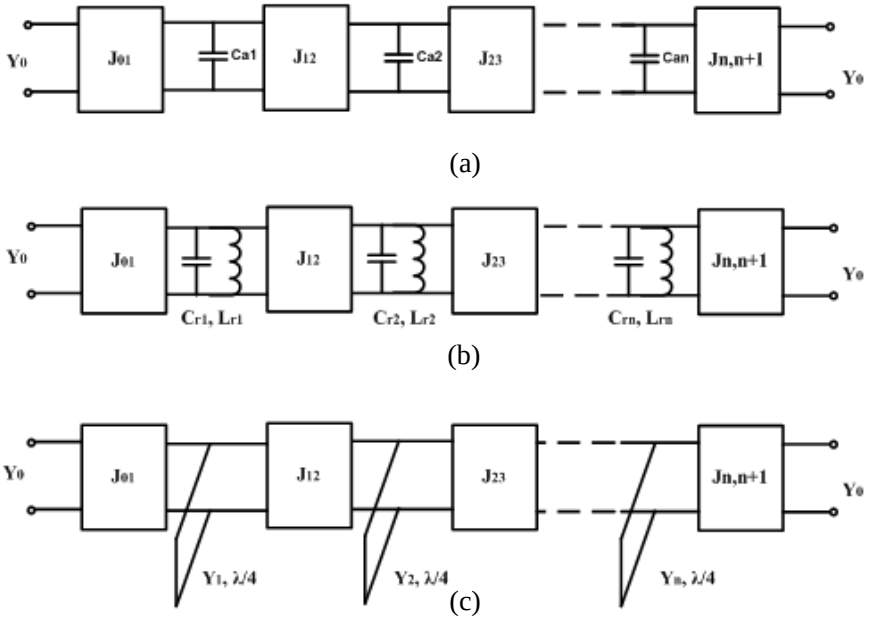

Figure 3. Lowpass to bandpass transformation. (a) Distributed lowpass prototype filter; (b) Coupled resonator bandpass filter achieved by a lowpass to bandpass transformation; (c) Shunt stub filter achieved by Richard's transformation.

$$C_{a,k+1} = \frac{J_{k,k+1}^2}{C_{a,k} g_k g_{k+1}} \quad k = 1, 2, \ldots, N-2 \tag{20}$$

Considering a bandpass filter with a center frequency of f_0 and a bandwidth of Δf, if it is in the form of Fig. 3(b) we will have an admittance slope for the kth resonator of

$$b_k = \frac{2C_{ak}}{\Delta\omega} = \frac{C_{ak}}{\pi\Delta f} \tag{21}$$

and the resonator elements are given by

$$C_{rk} = \frac{b_k}{2} \quad \text{and} \quad L_{rk} = \frac{1}{C_{rk}\omega_0^2} \tag{22}$$

If the bandpass filter is a shunt stub filter as in Fig. 3(c) we may use formulas listed on Page 153 of [21] to compute the characteristic impedance of each short-circuited stub, Z_{ck}. In order to have all the J

inverters at the same impedance level, we need to set the dimensional parameter h to be

$$h = \frac{g_2}{g_1}\left(\frac{J_{1,2}}{Y_0 g_0}\right)^2 \tag{23}$$

The design of the tri-band filter may be regarded as the design of three bandpass filters simultaneously. We can term the passbands centered at frequencies f_{r1}, f_{r2} and f_{r3} as passbands I, II, and III. The three bandpass filters are derived from one distributive lowpass prototype filter, and thus have the same number of poles and use common J inverters.

The tri-mode T-shape branches may be equalized to shunt-resonators with required admittance slopes at f_{r1}, f_{r2}, and $\lambda/4$ short circuited stub with required characteristic impedance at f_{r3}, hence realizing the tri-band filter.

If commensurate T-shape branches are used, passbands I and II will have the same bandwith because of equal admittance slopes at the resonating frequencies f_{r1} and f_{r2}. Also the frequency spacing between f_{r1} and f_{r3} will equal to that between f_{r2} and f_{r3}. Fig. 4 is the circuit of a 3-pole tri-band filter using three T-shape branches.

To design the parameters of the kth T-shape branch, we need to solve the following equations:

$$\frac{L\sqrt{\varepsilon_{eff}}(1+k_5)}{2\pi Z_1 c}\frac{(k_1k_3-3k_2k_4)+k_1k_4k_5+k_2k_3/k_5}{(k_3-k_4k_5)^2} = \frac{C_{ak}}{\pi\Delta f_{1,2}} \tag{24}$$

$$\frac{Z_1^2}{Z_1+Z_o} = Z_{ck} \tag{25}$$

$$\theta_{r1} = \pi - \theta_{r2} = \frac{\pi f_{r1}}{2f_{r3}} = \arctan\left(\sqrt{\frac{Z_1 Z_o}{Z_s(Z_1+Z_o)}}\right) \tag{26}$$

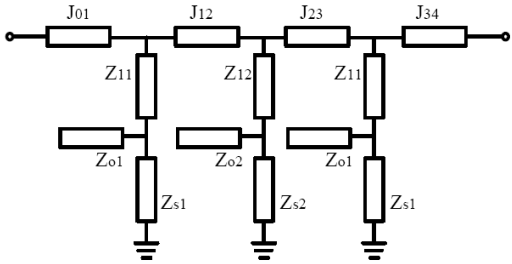

Figure 4. Circuit topology of a three-pole tri-band filter with three T-shape branches.

(24) gives the relationship between the admittance slopes of resonators and the bandwidth for passbands I and II. (25) relates the equivalent characteristic impedances of shunt stubs for passband III, and (26) gives the ratios between the center frequencies.

Hence this is a multi-object problem, and because of its complexity, a genetic algorithm routine [23] was used to conduct a global search of the circuit parameters for each T-shape branch.

3. DESIGN EXAMPLE

To explain the design procedure a 3-pole tri-band filter design example is presented here, commencing from a 3rd order Chebyshev prototype filter with an in-band ripple of 0.01 dB. The three passbands are 600–900 MHz, 1350–1650 MHz and 2100–2400 MHz, with the center frequencies at 750 MHz, 1500 MHz and 2250 MHz.

The lumped lowpass prototype filter has element values:

$$g_0 = 1, \quad g_1 = g_3 = 0.6291, \quad g_2 = 0.9702, \quad g_4 = 1.$$

If we set the input and output impedance to be $50\,\Omega$, by using (17)–(20) we obtain the element values of the distributive lowpass filter as:

$$J_{01} = J_{12} = J_{23} = J_{34} = 1/Z_0 = 0.02\,\text{s};$$
$$C_{a1} = C_{a3} = 0.0126\,\text{F}, \quad C_{a2} = 0.0194\,\text{F}.$$

Using (21), we derive the admittance slopes of the three branches at f_{r1}, f_{r2} as

$$b_1 = b_3 = 0.01337\,(\text{s/GHz}), \quad b_2 = 0.02054\,(\text{s/GHz}).$$

For the 3rd passband, using the formula in [22], the characteristic impedances of the shunt stubs are:

$$Z_{c1} = Z_{c3} = 16.06\,\Omega \text{ and } Z_{c2} = 10.8\,\Omega$$

Table 1. Circuit parameters of a three-pole tri-band filter using commensurate T-shape branches.

Pole order, k	1, 3	2
b_k of Passband I, II (s/GHz)	0.01337	0.02054
Z_{ck} of passband III (Ω)	16.06	10.8
Z_1 (Ω)	41.1	27.1
Z_o (Ω)	65.3	40.9
Z_s (Ω)	30.9	20.1

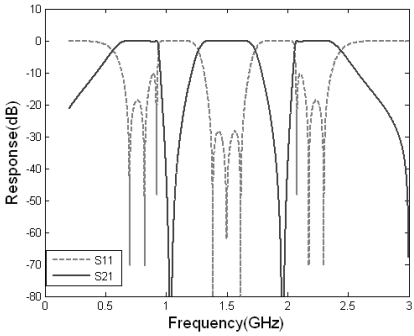

Figure 5. Circuit simulation result of the initial design for a three-pole tri-band filter with three T-shape branches.

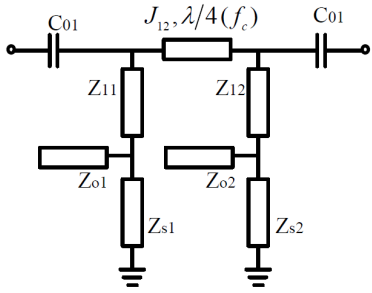

Figure 6. Two-port circuit to determine the transmission poles of each band by applying weak capacitive couplings at the two ports.

The circuit parameters obtained by using the genetic algorithm routine are given in Table 1.

Quarter wavelength transmission lines at f_{r3}, the center frequency of the three passbands, are used to implement the J inverters that connect the three T-shape branches.

A circuit simulation using Ansoft Serenade 8.7 [24] is conducted for validating the initial design, with the response shown in Fig. 5.

Checking the simulation result of the initial design carefully, we find that passband I and passband III each have poor return loss performance at the band edges close to passband II, with some shift of the required center frequencies. This is because the connecting lines are only narrow-band J inverters at passband III and are not equal to quarter-wave length at passbands I and II.

Figure 6 shows a sub-network, which contains two T-shape branches connected by a transmission line. Using weak capacitive couplings at the external ports and conducting a two-port simulation, two transmission poles from S_{21} plot are obtained, thus determining the coupling bandwidth. We may observe the variation of S_{21} when the length of the connecting line changes.

As seen in Fig. 7, a connecting line with a length unequal to a quarter-wave length may still act as a coupling element, but frequency shift for the two transmission poles are incurred compared with the case that uses quarter-wave length line. In this design, the connecting line (90° at 1.5 GHz) is longer than a quarter-wave length at passband II but shorter than that at passband I, resulting in downward frequency shift at the higher passband and upward frequency shift at

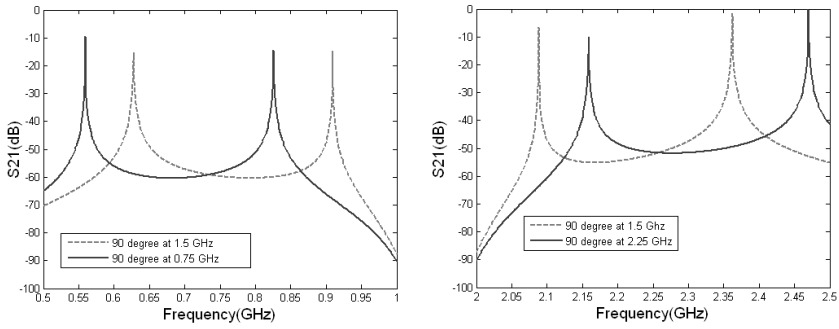

Figure 7. Compared two-port simulation results of a coupling structure using connecting lines of different lengths: (a) Passband I; (b) Passband II.

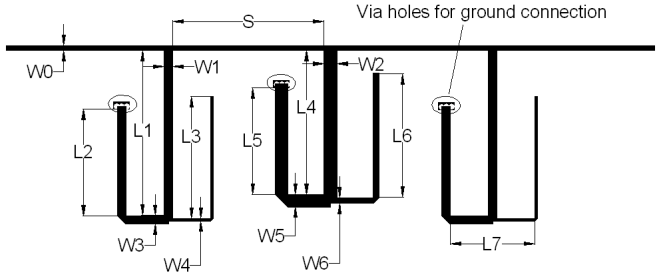

Figure 8. Circuit dimensions of the final design for a three-pole tri-band filter with three T-shape branches integrated inside. $W_0 = 0.92$; $W_1 = 1.67$; $W_2 = 2.43$; $W_3 = 1.57$; $W_4 = 0.4$; $W_5 = 2.36$; $W_6 = 1.05$; $S = 28.45$; $L_1 = 31$; $L_2 = 19.92$; $L_3 = 22.95$; $L_4 = 27.03$; $L_5 = 20.04$; $L_6 = 23.13$; $L_7 = 16$. (Unit: mm).

the lower passband. There will also be some slight changes giving some degradation of return loss in addition to inaccurate bandwidths for passbands I and II.

In practice, therefore, we need to do some optimization on widths and lengths of the lines in T-shape branches to tune the resonating frequencies and admittance slopes to compensate for these effects.

Figure 8 gives the final circuit of the tri-band filter. It is fabricated on Rogers 4003C material with a dielectric constant of 3.38 and a thickness of 0.4 mm. The folded T-shape branches realize the tri-band filter in an area no larger than a short-circuited stub filter.

The simulation results and measured results of the tri-band filter are shown in Fig. 9.

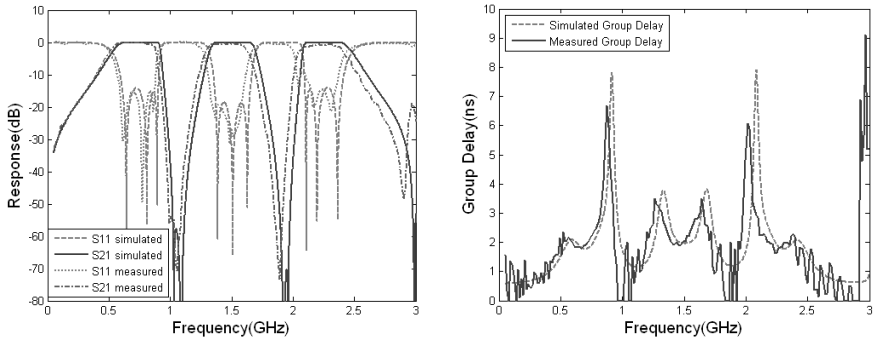

Figure 9. Comparison between measured and simulated result, of a tri-band filter using T-shape branches: (a) Amplituide response; (b) Group delay.

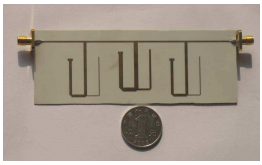

Figure 10. Photograph of the fabricated tri-band filter using T-shape branches.

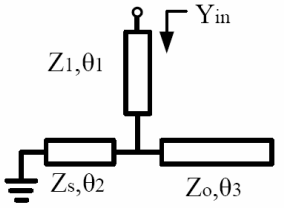

Figure 11. T-shape branch with non-commensurate transmission lines.

We observe that the lowest insertion loss for the three passbands, from the lowest to the highest, are 0.15, 0.5, and 0.7 dB, with return losses of better than 15 dB, 18 dB and 10 dB respectively. High isolation of more than 60 dB is achieved between the three passbands. There exists some frequency shift between measured and simulated passbands due to fabrication tolerances.

The example filter is shown in Fig. 10. Because of the existence of near-band transmission zeros between the passbands, asymmetrical amplitude response can be observed for passbands I and II.

4. TRI-BAND FILTERS WITH FULLY CONTROLLABLE PASSBANDS

A tri-band filter designed with commensurate T-shape branches has two limitations: the frequency spacing between f_{r1} and f_{r3} must equal that between f_{r2} and f_{r3}, and the 1st and 2nd passbands have the same bandwidth due to their equal admittance slope. To achieve controllable passbands without such limitations we need to allow the lengths of the three transmission lines to be different in the T-shape branch to obtain more design freedom.

We find

$$Y_{in} = \frac{j\left(\tan\theta_1 + \frac{Z_1}{Z_o}\tan\theta_3 - \frac{Z_1}{Z_s}\cot\theta_2\right)}{Z_1\left(1 + \frac{Z_1}{Z_s}\tan\theta_1\cdot\cot\theta_2 - \frac{Z_1}{Z_o}\tan\theta_1\cdot\tan\theta_3\right)} \tag{27}$$

To achieve three passbands with center frequencies of f_{r1}, f_{r2}, f_{r3}, and bandwidths of Δf_1, Δf_2, Δf_3, the kth T-shape branch will satisfy the following 6 equations:

$$Y_{in}(f_{rn}) = 0 \quad n = 1, 2, 3 \tag{28}$$

$$b(f_{rn}) = \frac{dB_{in}}{d\omega}|_{f=f_{rn}} = \frac{d(\mathrm{Im}(Y_{in}))}{d\omega}|_{f=f_{rn}} = \frac{C_{ak}}{\pi\cdot\Delta f_n} \quad n=1,2,3 \tag{29}$$

Here, we use a finite difference method to calculate $b(f_{rn})$ as:

$$b(f_{rn}) = \frac{dB_{in}}{d\omega}|_{f=f_{rn}} = \frac{d(\mathrm{Im}(Y_{in}))}{d\omega}|_{f=f_{rn}} \approx \frac{\mathrm{Im}(Y_{in}(f_{rn}+\delta)) - \mathrm{Im}(Y_{in}(f_{rn}))}{2\pi\delta} \tag{30}$$

where δ is a small variation of frequency.

(28) and (29) are a set of transcendental equations, which can not be easily solved analytically. Again, a genetic algorithm is used to solve the equation set to obtain the characteristic impedance and electrical length of each transmission line section in Fig. 4. To speed up the convergence in solving the multiple-objective problem, we should firstly eliminate the redundant unknowns by expressing them as functions of the other unknowns.

A practical and important issue in realizing a tri-band filter of this topology is the impedance level of each transmission line, which should be within a realizable range. If the kth T-shape branch has impedance levels of Z_{1k}, Z_{sk}, Z_{ok} and electrical lengths $\theta_{1k}, \theta_{sk}, \theta_{ok}$, then for the jth T-shape branch, the related parameters can be a good solution if they satisfy the following:

$$\frac{Z_{1k}}{Z_{1j}} = \frac{Z_{ok}}{Z_{oj}} = \frac{Z_{sk}}{Z_{sj}} = \frac{C_{aj}}{C_{ak}} \tag{31}$$

$$\theta_{1k} = \theta_{1j}; \quad \theta_{sk} = \theta_{sj}; \quad \theta_{ok} = \theta_{oj} \tag{32}$$

The maximum impedance ratio (MIR) in a T-shape branch can be defined as:

$$R_{\max,k} = \frac{\max(Z_{1k}, Z_{sk}, Z_{ok})}{\min(Z_{1k}, Z_{sk}, Z_{ok})} \tag{33}$$

and the overall maximum impedance ratio of all T-shape branches is:

$$R_{\max,o} = \frac{\max(Z_{1k}, Z_{sk}, Z_{ok})}{\min(Z_{1k}, Z_{sk}, Z_{ok})} \cdot \frac{\max(C_{ai}|i = 1, 2, \ldots, n)}{\min(C_{ai}|i = 1, 2, \ldots, n)} \tag{34}$$

From (31) know that for given center frequencies and bandwidths we can obtain the same MIR for all the T-shape branches, and it is possible to tune the impedance level of the kth T-shape branch by changing the value of C_{ak}. For the lowest $R_{\max,o}$, we should set:

$$C_{a1} = C_{a2} = \ldots = C_{an} \tag{35}$$

and then:

$$R_{\max,o} = R_{\max} \tag{36}$$

The impedance levels of each connection line are determined by the values of C_{a1}, C_{a2}, $C_{a3}, \ldots, C_{an}$. The MIR is a key factor in deciding the realizability of a specified tri-band filter. We can set the bandwidth ratios as: $R_1 = \Delta f_2/\Delta f_1$ and $R_2 = \Delta f_3/\Delta f_1$. If the center frequencies are given, we may obtain a plot of MIR with respect to the values of R_1 and R_2. Fig. 12 is a case where the three center frequencies are located at 0.85 GHz, 1.8 GHz and 2.25 GHz.

If we assume the realizable impedance range of the microstrip line to be $13 \sim 130\,\Omega$, the allowable MIR of a T-shape branch must be lower than 10. It may be observed from Fig. 12 that MIR is

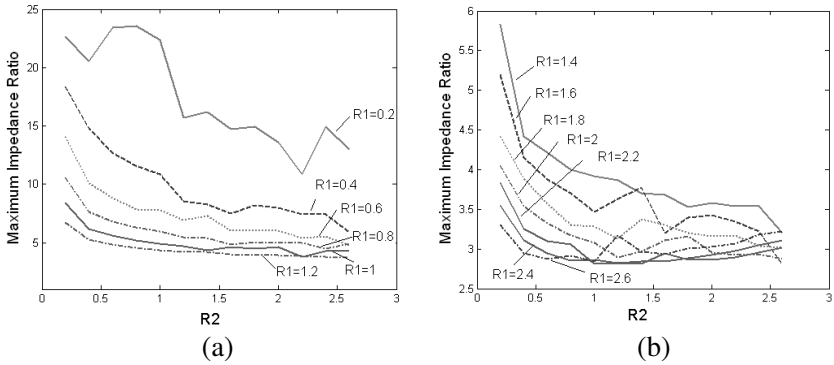

Figure 12. Maximum impedance ratio with respect to bandwidth ratios: (a) $0.2 \le R_1 \le 1.2$; (b), $1.4 \le R_1 \le 2.6$.

high when R_1 or R_2 is low, but in a large value range of R_1 and R_2 ($0.4 \leq R_1 \leq 2.6 \cap 0.4 \leq R_1 \leq 2.6$) the MIR is lower than 10, which means the tri-band filter is realizable without using extremely wide or narrow transmission lines.

Here we give a design example. For a 3-pole tri-band filter with passbands of 700–1000, 1650–1950, and 2200–2300 MHz, we set:

$$J_{01} = J_{34} = 1/Z_0 = 0.02$$

Then we find:

$$C_{a1} = C_{a3} = \frac{J_{01}^2 g_0 g_1}{Z_0} = 0.0126\,\mathrm{F}$$

To achieve the lowest overall MIR, we set:

$$C_{a2} = C_{a1} = 0.0126\,\mathrm{F}$$

Thus:

$$J_{12} = J_{23} = \sqrt{\frac{C_{a1}C_{a2}}{g_1 g_2}} = \frac{C_{a1}}{\sqrt{g_1 g_2}} = 0.0161\,\mathrm{s}$$

The genetic algorithm routine was used to derive the impedances and electrical lengths of all T-shape branches, as shown in Table 2. The circuit simulation result of the initial design is shown in Fig. 13, from which we can observe frequency shifting of the passbands and imperfect in-band return loss.

To compensate for the effects incurred by the approximation incurred by the imperfect J inverters, an overall performance

Pole order, k	1, 2, 3
C_{ak} (F)	0.0126
Z_{1k} (Ω)	29.77
θ_{1k} (degree)	91.3@1.5 GHz
Z_{sk} (Ω)	14.94
θ_{2k} (degree)	93.94@1.5 GHz
Z_{ok} (Ω)	105.11
θ_{3k} (degree)	67.04@1.5 GHz

Table 2. Circuit parameters of a three-pole tri-band filter using length-non-commensurate T-shape branches.

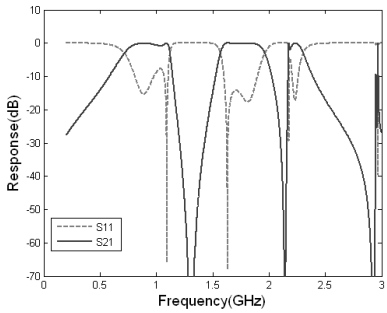

Figure 13. Circuit simulation result of initial design of the tri-band filter with asymmetric passbands.

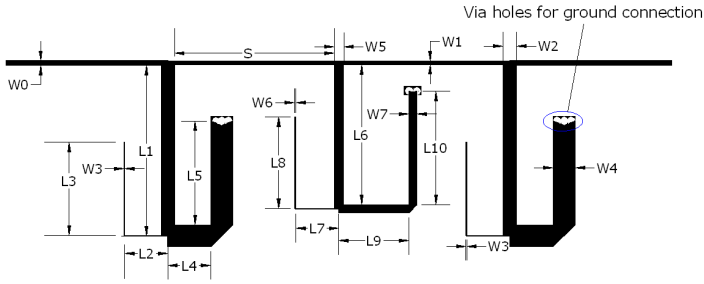

Figure 14. Circuit dimensions of the final design for a three-pole tri-band filter with three T-shape branches integrated inside. $W_0 = 0.92$; $W_1 = 0.64$; $W_2 = 2.57$; $W_3 = 0.13$; $W_4 = 4.07$; $W_5 = 1.77$; $W_6 = 0.19$; $W_7 = 1.51$; $S = 29.56$; $L_1 = 29.51$; $L_2 = 8$; $L_3 = 17.21$; $L_4 = 8$; $L_5 = 19.14$; $L_6 = 25.85$; $L_7 = 8$; $L_8 = 16.88$; $L_9 = 13$; $L_{10} = 20.95$. (Unit: mm).

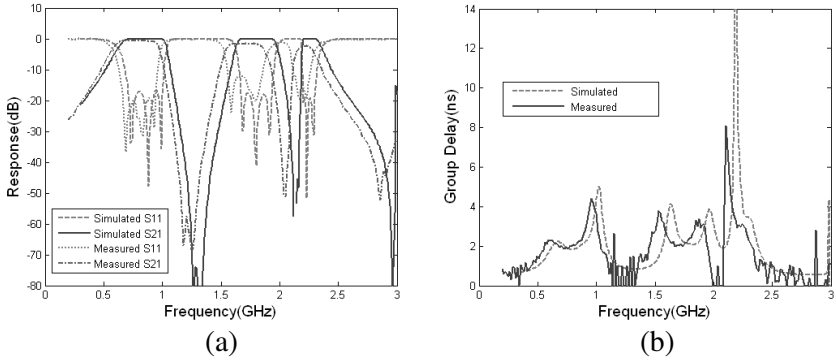

Figure 15. Compared results of the tri-band filter with asymmetric passbands: (a) Amplitude response; (b) Group delay.

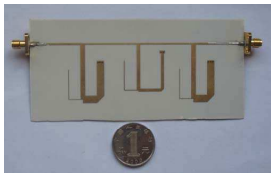

Figure 16. Photograph of the tri-band filter using non-commensurateT-shape branches.

optimization is conducted with only the circuit parameters of the T-shape branches being variables. Fig. 14 gives the circuit dimensions after optimization.

Comparisons between the circuit simulation and measured results are shown in Fig. 15, in which we observe frequency shifting incurred by fabrication tolerances. The lowest insertion loss of the three passbands, from lowest to highest, are 0.5 dB, 1.5 dB and 2.3 dB repectively. The return losses are better than −12 dB.

This design exhibits asymmetric performance in passband allocation and bandwidths. Fig. 16 shows a photograph of the filter.

Next, some detailed comparison between this work and other techniques as presented in [3, 17] and [20] are given. As can be seen in Table 3, T-shaped branch tri-band filters gives a greater

Table 3. Performance comparison between the proposed tri-band filter and other techniques.

Solution	This work	Ref. [3]	Ref. [17]	Ref. [20]
Technique Type	Tri-mode resonator	Dual behavior Resonator	Tri-section SIR	Tri-section SIR
Pole Number	3	2	2	2
Center Frequencies (GHz)	0.85/1.8/2.25	1.4/2.3/3.5	1/2.4/3.6	1/2.4/3.6
Bandwidths (MHz)	300/300/100	About 50/200/50	About 50	About 50
Ability of setting bandwidths	Yes	Not discussed	No	No
Impedance Range (Ω)	$16.5 \sim 124$	N/A	$50 \sim 93.3$	$50 \sim 93.3$
Insertion Loss (dB)	0.5/1.5/2.3	2.5/2.5/3	2.2/1.8/1.7	2/1.9/1.7
Isolation (dB)	70/40	50/50	40/30	40/25
Size (mm^2)	$120 * 44$	50 mm in length	$60 * 60$	$40 * 40$
Material Permittivity	3.38	9.9	2.65	2.45

range of bandwidths, and wideband bandwidths can be easily achieved compared with tri-section SIR techniques. Also the T-shape branch technique can achieve lower insertion loss. Because of the transmission zeros (there exist N zeros between every two nearest bands of a N-pole tri-band filter), the isolation between bands is much higher than all the other techniques, taking into account the bandwidths of the pass and stop bands. The relatively larger dimension of the example filter is due to the lower permittivity of the PCB material, lower center frequencies and higher number of poles. Also it is possible to achieve more compact dimensions using meandered connecting lines. As a shortcoming, the required impedance range of T-shape branch filters are wider than those in [17] and [20], but are still realizable with current PCB techniques.

5. CONCLUSIONS

A new tri-mode T-shape branch is introduced and used to design tri-band filters. A theoretical analysis of commensurate T-shape branches is given with a detailed design procedure, and an example filter fabricated and measured. Good agreement between simulation and measurement results has validated the theory. To achieve arbitrary passbands, non-commensurate T-shape branches are proposed to give more design freedom, and a genetic algorithm is used. Design example with measured results have shown the realizability of arbitrary center frequencies and bandwidths. By deriving the three passbands from one distributive lowpass prototype filter, one needs only to tune the admittance slope of each resonating mode to control the bandwidths.

ACKNOWLEDGMENT

The authors would like to thank Dr. Ralph Levy for valuable comments and grammatical improvements, and Dr. Hongfu Meng of Southeast University for discussions.

REFERENCES

1. Lin, Y.-S., C.-C. Liu, K.-M. Li, and C.-H. Chen, "Design of an LTCC tri-band transceiver module for GPRS mobile applications," *IEEE Trans. Microw. Theory Tech.*, Vol. 52, No. 12, 2718–2724, Dec. 2004.
2. Mokhtaari, M., J. Bornemana, K. Rambabu, and S. Amari, "Coupling matrix design of dual and triple passband filters,"

IEEE Trans. Microw. Theory Tech., Vol. 54, No. 11, 3940–3945, Nov. 2006.

3. Quendo, C., E. Rius, A. Manchec, Y. Clavet, B. Potelon, J.-F. Favennec, and C. Person, "Planar tri-band filter based on dual behaviour resonator (DBR)," *Proc. Eur. Microw. Conf.*, 269–272, Oct. 1995.
4. Liu, Y. and W.-B. Dou, "A dual-band filter realized by alternately connecting the main transmission-line with shunt stubs and shunt serial resonators," *IEEE Microw. Wireless Compon. Lett.*, Vol. 19, No. 5, 296–298, May 2009.
5. Chen, X.-P., K. Wu, and Z.-L. Li, "Dual-band and triple-band substrate integrated waveguide filters with chebyshev and quasi-elliptic responses," *IEEE Trans. Microw. Theory Tech.*, Vol. 55, No. 12, 2569–2578, Dec. 2007.
6. Zhao, H. and T. J. Cui, "Novel triple-mode resonators using split-ring resonator," *Microw. Opt. Technol. Lett.*, Vol. 49, No. 12, 2918–2922, Dec. 2007.
7. De Paco, P., O. Menendez, and J. Marin, "Dual-band filter using non-bianisotropic split-ring resonators," *Progress In Electromagnetics Research Letters*, Vol. 13, 51–58, 2010.
8. Wu, G.-L., W. Mu, X.-W. Dai, and Y.-C. Jiao, "Design of novel dual-band bandpass filter with microstrip meander-loop resonator and CSRR DGS," *Progress In Electromagnetics Research*, Vol. 78, 17–24, 2008.
9. Wang, X.-H. and B.-Z. Wang, "Compact broadband dual-band bandpass filters using slotted ground structures," *Progress In Electromagnetics Research*, Vol. 82, 151–166, 2008.
10. Wu, M.-S., Y.-Z. Chueh, J.-C. Yeh, and S.-G. Mao, "Synthesis of triple-band and quad-band bandpass filters using lumped-element coplanar waveguide resonators," *Progress In Electromagnetics Research B*, Vol. 13, 433–451, 2009.
11. Chen, F. C. and Q. X. Chu, "Tri-band bandpass filters using stub loaded resonators," *Electron. Lett.*, Vol. 44, No. 12, 747–749, Jun. 2008.
12. Lin, W.-J., C.-S. Chang, J.-Y. Li, D.-B. Lin, L.-S. Chen, and M.-P. Houng, "A new approach of dual-band filters by stepped impedance simplified cascaded quadruplet resonators with slot coupling," *Progress In Electromagnetics Research Letters*, Vol. 9, 19–28, 2009.
13. Chen, C. F., T. Y. Huang, and R. B. Wu, "Design of dual- and triple-passband filters using alternately cascaded multiband

resonators," *IEEE Trans. Microw. Theory Tech.*, Vol. 54, No. 9, 3550–3558, Sep. 2006.

14. Lee, C. H., C. I. G. Hsu, and H. K. Jhuang, "Design of a new tri-band microstrip BPF using combined quarter- wavelength SIRs," *IEEE Microw. Wireless Compon. Lett.*, Vol. 16, No. 11, 594–596, Nov. 2006.
15. Hsu, C.-I. G., C.-H. Lee, and H.-K. Jhuang, "Design of a novel quadband microstrip BPF using quarter-wavelength stepped-impedance resonators," *Microw. J.*, Vol. 50, No. 2, 102–112, Feb. 2007.
16. Chen, F. C. and Q. X. Chu, "Design of compact tri-band bandpass filters using assembled resonators," *IEEE Trans. Microw. Theory Tech.*, Vol. 57, No. 1, 165–171, Jan. 2009.
17. Lin, X. M. and Q. X. Chu, "Design of triple-band bandpas filter using tri-section stepped-impedance resonators," *Proc. Int. Microw. Millimeter Wave Tech. Conf.*, 798–800, Guilin, China, Apr. 2007.
18. Chen, Y.-C., Y.-H. Shieh, C.-H. Her, and C.-I. G. Hsu, "Tri-band microstrip BPF design using tri-section SIRs," *IEEE AP-S Int. Symp. Dig.*, 3113–3116, Jun. 2007.
19. Hsu, C.-I. G., C.-H. Lee, and Y.-H. Hsieh, "Tri-band bandpass filter with sharp passband skirts designed using tri-section SIRs," *IEEE Microw. Wireless Compon. Lett.*, Vol. 18, No. 1, 19–21, Jan. 2008.
20. Chu, Q. X. and X. M. Lin, "Advanced triple-band bandpass filter using tri-section SIR," *Electron. Lett.*, Vol. 44, No. 4, 295–296, Feb. 2008.
21. Ma, Z., T. Shimizu, Y. Kobayashi, T. Anada, and G. Hagiwara, "Novel compact dual-band bandpass filters using composite resonators to obtain separately controllable passbands," *2006 Asia-Pacific Microwave Conference Proceedings*, Vol. 3, 1814–1817, FR4B-4, Dec. 2006.
22. Hong, J.-S. and M. J. Lancaster, *Microstrip Filter for RF/Microwave Applications*, Wiley, New York, 2001.
23. Holland, J. H., *Adaption in Natural and Artificial Systems*, MIT Press, Cambridge, MA, USA, 1992.
24. Ansoft Serenade 8.7, Ansoft Corporation.